Asian Journal of Chemistry; Vol. 37, No. 10 (2025), 2366-2378
ASIAN JOURNAL OF CHEMISTRY
https://doi.org/10.14233/ajchem.2025.34165

Synthesis, Spectroscopic, Electronic Charge Transfer and Non-covalent Interactions Studies on (*E*)-5-Bromo-3-((3-chloro-4-fluorophenyl)imino)indolin-2-one: *In vitro* Studies against the Cancer Cell Lines

S. REKHA[1,*], S. TAMILSELVAN[1,*], MOHD ASIF[2], MALIK NASIBULLAH[2], J.N. CHEERLIN MISHMA[3], P. MANIKANDAN[1] and S. KALEESWARAN[4]

[1]Department of Physics Arignar Anna Government Arts College, Cheyyar-604407, India
[2]Medicinal Chemistry Laboratory-ICEIR, Department of Chemistry, Integral University, Lucknow-226026, India
[3]Department of Physics, Rohini College of Engineering and Technology, Palkulam, Kanyakumari-629702, India
[4]Department of Physics, Madras Christian College, East Tambaram, Chennai-600059, India

*Corresponding authors: E-mail: rekhasowri@gmail.com; tamilraji1977@gmail.com

Received: 4 June 2025 *Accepted*: 23 August 2025 *Published online*: 30 September 2025 AJC-22119

This research focuses on synthesising an anticancer drug titled (*E*)-5-bromo-3-((3-chloro-4-fluorophenyl)imino)indolin-2-one (5BFIO) and validating its analytical values through theoretical and experimental evaluation using techniques such as FT-IR, FT-Raman, ^{1}H and ^{13}C NMR. Moreover, the anticancer activity of 5BFIO molecule was evaluated using molecular docking against cancer proteins (4B55, 5KYG and 6UGR) and 60 human cancer cell lines of NCI-60 under *in silico* and *in vitro* analyses, respectively. In the formation of docked complexes, low binding affinities -5.78 for 5BFIO-4B55, -6.72 for 5BFIO-5KYG and -8.86 for 5BFIO-6UGR) were noted in kcal/mol, respectively. Moreover, 5BFIO showed the best activity (49.59% GI) against the MCF7 breast cancer cell line. Density functional theory (DFT) was effectively employed to analyse the molecule's stability under optimal conditions for comparative studies that incorporate both observational and computational data from gas phases. The outcomes of this study present a comprehensive analysis of gas-phase properties, including nonlinear optical (NLO) behaviour, molecular electrostatic potential (MEP), electron localization function (ELF), localized orbital locator (LOL) and reduced density gradient (RDG) descriptors. The pharmacological evaluation demonstrated significant anticancer activity and it could be derivatized into a more potent drug-like molecule using chemical reactions.

Keywords: Spectroscopic studies, Electronic charge transfer, Non-covalent interactions, Molecular docking, Cancer cell lines.

INTRODUCTION

The imine functions of the Schiff bases have conveyed an interesting role in medicinal chemistry owing to interactions among the targeted amino acid residues of the proteins. Functionalized imine-containing compounds have been widely used in the treatment of various carcinomas, with several drug-like molecules receiving approval from the FDA [1,2]. On the contrary, oxindole containing compounds were also used in the treatment of cancer. Therefore, we synthesized a functionalized novel hybrid oxindole-imine-containing compound as an anticancer agent. The UV-Vis, FT-IR and (^{1}H and ^{13}C) NMR tools were utilized for the characterization of the synthesized material hybrid oxindole-imine-derivative compound. Furthermore, these spectra were validated through density functional theory (DFT) calculations to confirm the proposed molecular framework. Moreover, the characteristic energy of the synthesized molecule [(*E*)-5-bromo-3-((3-chloro-4-fluorophenyl)imino)indolin-2-one (5BFIO)] in its HOMO-LUMO form was also calculated. The stability of the compound was examined utilizing (NBO) analysis. Furthermore, the topological studies on electron localization function (ELF), localized orbital locator (LOL) and reduced density gradient (RDG) descriptors were also conducted.

Molecular docking methodology was utilized to elucidate the specific interactions between ligands and protein structures. After the *in silico* analysis, the proposed anticancer drug molecule was successfully evaluated by the NCI against 60 human cancer cell lines under *in vitro* investigation [3-6]. Drug-likeness, ADMET properties, binding energies from molecular docking, and anticancer activity suggest that this molecule holds significant potential for the treatment of

various malignancies. This can be achieved by making more effective changes to its structure through chemical processes.

EXPERIMENTAL

Synthesis process: The synthesis of oxindole-imine-containing compound 5BFIO molecule was achieved by the nucleophilic elimination reaction, whereby 5-bromodioxindole (**1**) was treated with the active arylamination in the presence of oxalic acid as sole catalyst. The formation of the imine (>C=N) functional group at room temperature within 21 min was significantly facilitated by the catalyst. Subsequently, the crude product as yellow precipitate was obtained and purified by column chromatography using ethyl acetate and *n*-hexane (**Scheme-I**).

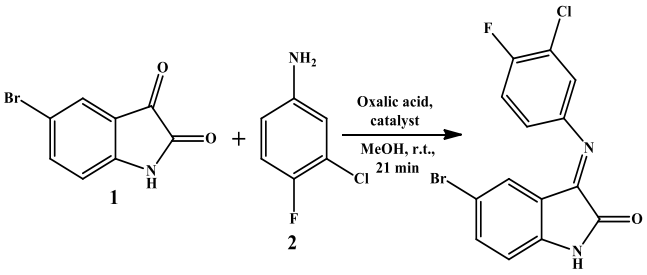

Scheme-I: Synthesis route of 5BFIO compound

Characterization: The IR and Raman spectra were examined using Agilent Cary 630 and Bruker RFS at range of 4000-450 and 4000-100 cm^{-1}, respectively. The Bruker AVIII 400 MHz spectrophotometer was used to acquire ^{13}C and ^{1}H NMR readings in DMSO-d_6 solvent.

Computational details: The optimized structure was calculated utilising Gaussian 09W [7] & Gauss view 6 [8] by the method of B3LYP and 6–311++G(d,p) basis set [9]. In the vibrational investigation, the (PED) of the molecule were standardized through VEDA [10], with a factor of scaling of 0.961 [11]. The bond length (BL) and bond angle (BA) were calculated by employing the CHEMCRAFT tool [12] and the framework has been optimized. NBO method was used to assess the interaction of orbitals [13-15]. Electron excitement and topological investigations were conducted using the Multiwfn [16] programme. An investigation was carried out on the properties of medications and their lipophilicity utilizing the SwissADME [17]. The research on molecular docking was performed using Patch Dock Tools [18].

RESULTS AND DISCUSSION

Geometry optimization: The 5BFIO molecule was evaluated through computational methods, as shown in Fig. 1 and the calculated values are summarized in Table-1. The titled molecule consists of 50 bond angles and 30 bond lengths.

TABLE-1
OPTIMIZED GEOMETRICAL PARAMETERS OF 5BFIO MOLECULE

Bond length (Å)	B3LYP/6-311++G(d,p)	Bond length (º)	B3LYP/6-311++G(d,p)	Bond length (º)	B3LYP/6-311++G(d,p)
N1-C9	1.462	N1-C9-C4	111	C8-C7-H23	120
C2-C3	1.517	N1-C9-C8	129	C7-C8-C9	120
C2-O10	1.208	C9-N1-H21	127.3	C7-C8-H24	120
C3-C4	1.42	C3-C2-O10	129.4	C9-C8-H24	120
C3-N11	1.358	C2-C3-C4	111	N11-C12-C13	120
C4-C5	1.42	C2-C3-N11	120	N11-C12-C17	120
C4-C9	1.42	C4-C3-N11	120	C13-C12-C17	120
C5-C6	1.42	C3-C4-C5	129	C12-C13-C14	120
C5-H22	1.1	C3-C4-C9	111	C12-C13-H25	120
C5-H27	1.002	C3-N11-C12	115	C12-C17-C16	120
C6-C7	1.421	C5-C4-C9	120	C12-C17-H22	135.8
C6-Br20	1.881	C4-C5-C6	120	C12-C17-H27	120
C7-C8	1.42	C4-C5-H22	120	C14-C13-H25	120
C7-H23	1.1	C4-C5-H27	83.8	C13-C14-C15	120
C8-C9	1.42	C4-C9-C8	120	C13-C14-Cl19	120
C8-H24	1.1	C6-C5-H22	120	C15-C15-Cl19	120
N11-C12	1.358	C6-C5-H27	138.5	C14-C15-C16	120
C12-C13	1.42	C5-C6-C7	120	C14-C15-F18	120
C12-C17	1.42	C5-C6-Br20	120	C16-C15-F18	120
C13-C14	1.42	H22-C5-H27	50.5	C15-C16-C17	120
C13-H25	1.1	C5-H22-C17	128.4	C15-C16-H26	120
C14-C15	1.42	C5-H27-C17	112.5	C17-C16-H26	120
C14-Cl19	1.719	C7-C6-Br20	120	C16-C17-H22	82.8
C15-C16	1.42	C6-C7-C8	120	C16-C17-H27	120
C15-F18	1.32	C6-C7-H23	120	H22-C17-H27	53.3
C16-C17	1.42				
C16-H26	1.1				
C17-H22	0.838				
C17-H27	1.1				
N1-H21	1.05				

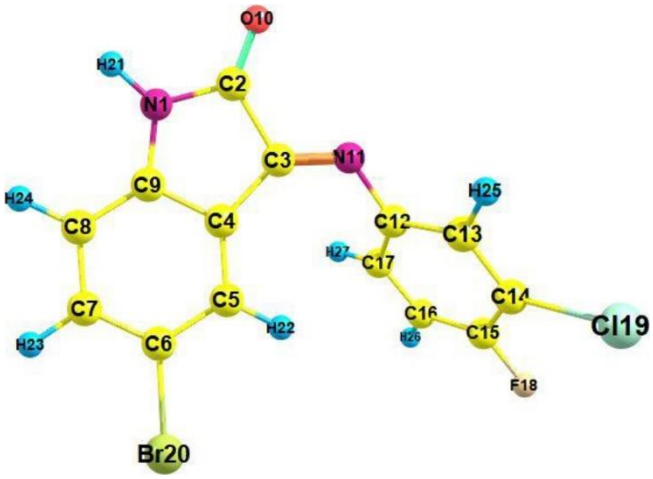

Fig. 1. Optimized structure of 5BFIO compound

The bond length at C6-Br20 = 1.881 is larger due to its homonuclear nature. The greatest length of bonds between carbon atoms in the C14-C19 range was determined to be 1.719Å. BL among the C2-C3 atoms was measured to be 1.517 Å, which was given the next highest priority. Such bonds might hold higher values, on the other hand, C17-H22 exhibits a lesser BL of 0.838 Å. The bond angle of C4–C5–H27 was the lowest at 83.8º, whereas that of C6–C5–H27 was the highest at 138.5º.

Vibrational analysis: Various functional groups present in the titled molecule were identified using vibrational spectroscopy [19]. A scaling value of 0.961 was employed. The examination of the molecule given involves 27 atoms and encompasses 75 regular vibrational modes. Fig. 2 shows the experimental FT-IR and FT Raman spectra. Table-2 presents the computed vibrational frequencies and their corresponding (PED).

C-C vibration: In the 1650-1200 cm^{-1} range, vibrations associated with the C–C stretching are clearly evident [20]. The computational frequencies were detected at 1583, 1654, 1550, 1245 and 1226 cm^{-1}, respectively. The experimental IR were observed at 1587 and 1284 cm^{-1} and FT Raman were detected at 1589 and 1264 cm^{-1}, respectively.

C–H vibration: Typically, the C–H symmetric vibrations occur between 3300 and 3000 cm^{-1} [21]. In the FTIR spectrum, a strong peak was observed at 3073 cm^{-1}, while the theoretical C–H vibrational modes with 99–100% PED contributions appeared at 3103, 3084, 3080, 3077, 3064 and 3059 cm^{-1}. All the estimated wavenumbers for 5BFIO molecule fell within the predicted range.

N-H vibration: The anticipated vibrational peaks for the N-H stretching mode are expected to appear within the range of 3500 to 3300 cm^{-1} [22]. For compound 5BFIO, the theoretical value for this vibrational frequency is predicted to be at 3498 cm^{-1}, with a contribution from the potential energy distribution (PED) calculated to be 100%.

C-N vibrations: Identifying the C-N stretching frequency in the side chains is challenging due to overlap with other vibrations. Kahovec & Kohlrausch [23] reported the C=N band's stretching vibration in salicylic aldoxime at 1617 cm^{-1}. The title compound exhibits a computed C=N stretching vibration at 1653 cm^{-1}, while experimental values were observed at 1621 cm^{-1} in the IR spectrum and 1606 cm^{-1} in the Raman spectrum.

O-C vibrations: The CO typically vibrates at a primary frequency between 1850 and 1550 cm^{-1} [24]. In experimental IR analyses, the 5BFIO vibrations were observed at 1751 cm^{-1}. Theoretical calculations predict the C=O stretching vibration at 1755 cm^{-1}, corresponding to 83% of the potential energy distribution (PED).

MEP analysis: Fig. 3 illustrates an arrangement of the MEP in the gas phase. Within MEP surfaces, the colour red and yellow signify regions with an abundance of electrons, which promote electrophilic attacks. Green represents neutral sites, while blue signifies areas with a deficiency of electrons that are favourable for nucleophilic attacks [25,26]. On transitioning from a gaseous state Moreover, it includes a coloured zone from -6.869 to 6.869 e^{-2} (gas).

NBO analysis: Table-3 summarizes the calculation of stabilized interaction at donor-acceptor levels. Maximum stabilized energies between LP1-N1 to π* C2-O10 with equilibrium energy 50.37 Kcal/mol, which is followed by LP1-N1 to π*C8-C9 with 39.07 Kcal/mol. For LP2-O10 to σ*N1-C2 is 28.19 kcal/mol, whereas σC17-H27 to σ*C17-H27 has a stabilized energy of 27.06 kcal/mol. At π*C14-C15 to π*C16-C17, πC4-C5 to π*C8-C9 and LP2-O10 to σ*C2-C3 stabilized energy to be 22.12, 22.77and 22.97 kcal/mol.

FMO analysis: In present investigation, the ring of phenyl is the LUMO area, with a corresponding energy of -0.245 eV, while the HOMO over 5-bromoindolin-2-one has an energy of -0.116 eV. The computed gap in energies in the gas phase is 3.504 eV. Fig. 4 shows the HOMO-LUMO plot and Table-4

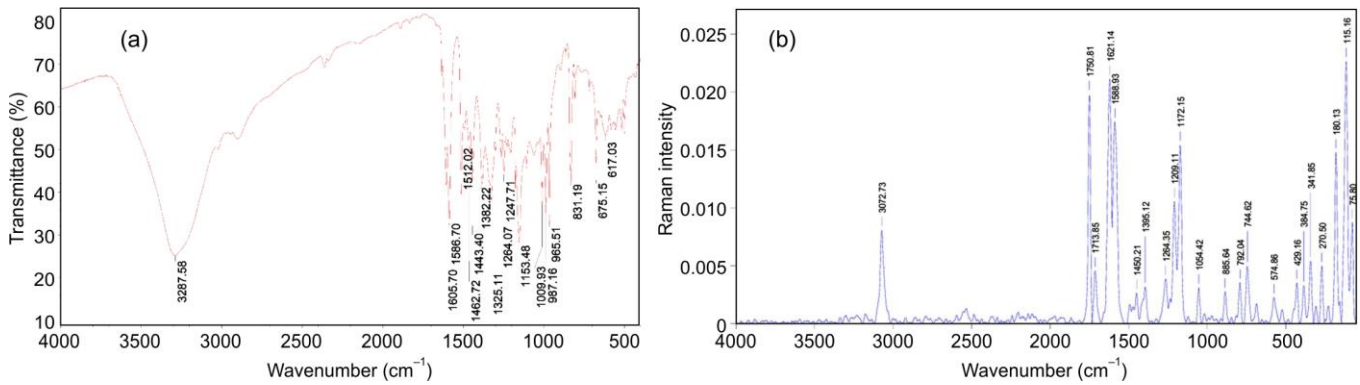

Fig. 2. Experimental (a) FT-IR and (b) FT-Raman spectrum of 5BFIO molecule

TABLE-2
VIBRATIONAL ASSIGNMENT OF 5BFIO MOLECULE

Mode	Experimental frequency		Theoretical frequency		IR intensity		Raman activity		[d]PED assignment (%)
	IR	Raman	Unscaled	Scaled[a]	IR	IA[b]	RR	RA[c]	
75			3640	3498	77	16		16	νNH (100)
74			3229	3103	2	0	37	3	νCH (100)
73			3209	3084	1	0	63	5	νCH (99)
72			3205	3080	1	0	165	12	νCH (99)
71		3073	3202	3077	0	0	121	9	νCH (99)
70			3188	3064	2	0	38	3	νCH (99)
69			3183	3059	7	1	132	10	νCH (100)
68		1751	1826	1755	476	100	71	5	νOC (83)
67	1606	1621	1725	1653	92	19	1375	100	νNC (79)
66	1587	1589	1647	1583	152	32	244	18	νCC (54)
65			1628	1564	30	6	535	39	νCC (51)
64			1613..36	1550	0	0	22	2	νCC (50)
63	1512		1605	1543	17	4	13	1	νCC (47) + βCCC (23)
62	1463	1450	1515	1456	197	41	44	3	βHCC (48)
61	1443		1490	1432	170	36	46	3	βHCC (59)
60			1462	1405	84	18	10	1	νCC (52) + βHNC (11)
59	1382	1395	1420	1365	5	1	7	0	νCC (38) βHCC (15)
58	1325		1403	1349	34	7	93	7	ννCC (12) + νNC (14) + βHNC (29) + βHCC (20)
57	1264		1309	1258	37	8	42	3	νCC (40) + βHCC (16)
56			1306	1255	59	12	17	1	νCC (34) + βHCC (13)
55	1248	1264	1296	1245	1	0	31	2	νCC (51)
54			1280	1230	11	2	54	4	νNC (16) + νCC (15) + νβHCC (38)
53			1276	1226	88	18	63	5	νCC (12)
52		1209	1260	1211	49	10	9	1	νNC (22) + βHNC (28) + βHCC (14)
51			1229	1181	46	10	31	2	νNC (14) + νFC (10) + βHCC (38)
50	1153		1196	1150	143	30	29	2	βHCC (27) + νNC (19)
49		1172	1164	1118	30	6	287	21	νNC (19) + νCC (11)
48			1148	1104	14	3	4	0	βHCC (61) + νCC (15)
47		1054	1132	1088	49	10	16	1	νCC (29) + βHCC (11) + βCCC (14)
46			1081	1039	14	3	15	1	νCC (48) + βHCC (32)
45	1010		1066	1025	21	4	14	1	βCCC (50)
44	966		1003	964	2	0	22	2	βCCN (21)
43			959	922	0	0	0	0	τHCCC (41) + τHCCN (27) + τCCCC (14)
42			955	918	1	0	4	0	τHCCC (72) + τCCCC (15)
41		886	925	889	33	7	9	1	βCCC (17) + νClC (1) + νNC (11)
40			915	879	3	1	1	0	τHCCC (72)
39			894	860	20	4	4	0	βCCC (10) + τHCCC (37)
38	831		891	856	8	2	25	2	βCCC (15) + τHCCC (30)
37			834	802	31	7	10	1	τHCCC (73)
36		792	827	794	35	7	1	0	τHCCC (34) + τHCCN (54)
35			803	772	14	3	12	1	τCCCN (13) + ωONCC (35) + ωNCCC (13)
34			802	771	28	6	51	4	βCCC (20) + βFC (14)
33		745	753	724	27	6	14	1	βCCC (17)
32			733	704	3	1	1	0	τCCCC (48) + τCNCC (12) + ωONCC (16)
31			717	689	9	2	3	0	τCCCC (10)
30	675		706	679	9	2	8	1	τCCCC (26)
29			693	666	3	1	13	1	νBrC (10) + βCCC (15) + βOCN (10) + βCNC (13)
28	617		648	622	5	1	3	0	βNCC (15) + βOCN (17)
27			627	603	14	3	9	1	ωClCC (14) + ωNCCC (18)
26		575	615	591	13	3	26	2	βNCC (10) + τCCNC (20) + ωONCC (15)
25			567	545	11	2	3	0	ωNCCC (18)
24			539	518	8	2	5	0	βNCC (13) + βFCC (10)
23			534	513	21	4	6	0	νCC (10) + νBrC (11) + βCNC (19) + νNC (14)
22			512	492	72	15	12	1	τHNCC (23) + βFCC (17)
21			501	481	8	2	2	0	νClC (10) + βFCC (14) + βCCC (10)

20		461	443	18	4	1	0	τHNCC (24) + τCCCC (13)
19	429	443	426	19	4	24	2	τHNCC (23) + τCCCC (15) + ωNCCC (11)
18		418	402	6	1	16	1	τCCCC (20)
17	385	394	379	5	1	4	0	νClC (14) + τCCCC (22)
16		376	361	5	1	1	0	τCCCC (60) + τCNCC (12) + τONCC (16)
15	342	340	327	3	1	4	0	ωFCCC (10)
14		321	308	2	0	9	1	ωFCCC (10) + βBrC (11)
13		306	294	2	0	8	1	τCCCC (16) + ωBrCCC (36) + ωNCCC (19)
12	271	274	263	1	0	11	1	βNCC (15) + βFCC (17)
11		237	228	1	0	3	0	νBrC (45)
10		209	201	1	0	5	0	βClCC (30)
9	180	188	180	0	0	10	1	βClCC (23) + βBrCC (14)
8		161	155	2	0	5	0	βCNC (12) + βClCC (13) + τCCCC (19) + ωClCCC (19)
7		144	138	0	0	0	0	τCCCC (26) + ωClCCC (24)
6		121	116	2	0	13	1	τCCCN (10) + τCCCC (50)
5	115	115	110	0	0	5	0	βCCC (14) + βCCN (12) + βBrCC (28) + τCCCC (12)
4	76	78	75	1	0	3	0	βNCC (12) + τCNCC (14) + τCCCC (11) + τCCNC (13)
3		43	41	0	0	4	0	βCNC (21) + τCNCC (16) + τCCCC (12) + ωNCCC (20)
2		34	33	1	0	4	0	τCCCN (17) + τCCNC (18)
1		15	14		0	10	1	τCNCC (55) + βCNC (17)

[a]Scaling factor: 0.961 for B3LYP/6-311++G(d,p). [b]Relative IR absorption normality intensities with highest peak absorption equal to 100. [c]Relative Raman intensities normalized to 100. [d]γ-stretching, β-Bending, τ-Torsion, ω- out of plane.

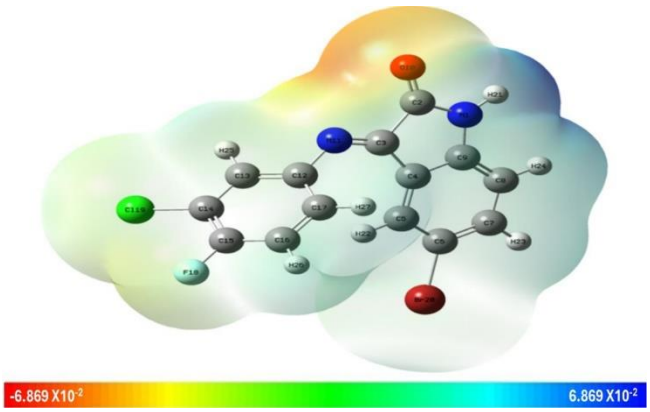

Fig. 3. MEP plot of 5BFIO in gas phase

lists the computed parameters. The outcomes are below 5 eV, aligning with the characteristics of bioactive materials. This indicates that 5BFIO has greater stability in the gaseous phase. Furthermore, its softness, combined with non-toxicity, suggests broad versatility, making it a promising candidate for applications ranging from pharmaceuticals to industrial processes.

NLO activity: For applications in photonics and materials science, the combination of DFT and NLO analysis is a potent tool for comprehending and forecasting the optical behaviour of materials [27]. The α, β and μ values of 5BFIO are shown in Table-5. The obtained dipole moment (μ) in the gas phase was 2.16954 D, with a computed value of 3.33×10^{-23} esu and the first hyperpolarizability (β) was calculated as 1.1608×10^{-30} esu. Higher β values for 5BPIO enhance its NLO

TABLE-3
SECOND-ORDER FOCK MATRIX (NBO) ANALYSIS

Donor (i)	ED/e	Acceptor (j)	ED/e	$E^{(2)}$ (kJ/mol)[a]	E(j)-E(i) (a.u.)[b]	F(i,j) (a.u.)[c]
LP1-N1	1.67406	π*C2-O10	0.11431	50.37	0.29	0.111
LP1-N1	1.67406	π*C8-C9	0.18225	39.07	0.29	0.096
LP2-O10	1.84267	σ*N1-C2	0.04229	28.19	0.67	0.125
σC17-H27	1.97952	σ*C17-H27	0.00591	27.06	4.7	0.319
LP2-O10	1.84267	σ*C2-C3	0.05119	22.97	0.61	0.107
πC4-C5	1.65856	π*C8-C9	0.18225	22.77	0.28	0.072
π*C14-C15	0.4428	π*C16-C17	0.17297	22.12	0.32	0.119
πC16-C17	1.69677	π*C12-C13	0.19137	20	0.28	0.069
πC16-C17	1.69677	π*C14-C15	0.22634	19.84	0.27	0.067
LP3-F18	1.9245	π*C14-C15	0.22634	19.09	0.42	0.088
πC4-C5	1.65856	π*C3-N11	0.07715	17.39	0.29	0.067
πC4-C5	1.65856	π*C6-C7	0.18996	17.19	0.27	0.062
LP1-N11	1.85091	σ*C3-C4	0.02481	15.12	0.79	0.1
LP3-Cl19	1.92328	π*C14-C15	0.22634	13.28	0.32	0.064
LP1-N11	1.85091	π*C12-C13	0.19137	12.13	0.36	0.063
σC17-H27	1.97952	π*C16-C17	0.17297	10.95	0.84	0.094
πC3-N11	1.89898	π*C2-O10	0.11431	9.44	0.36	0.054
σC2-C3	1.96481	σ*N11-C12	0.01443	5.61	1.07	0.069
σC2-C3	1.96481	σ*C4-C5	0.01273	4.41	1.18	0.065

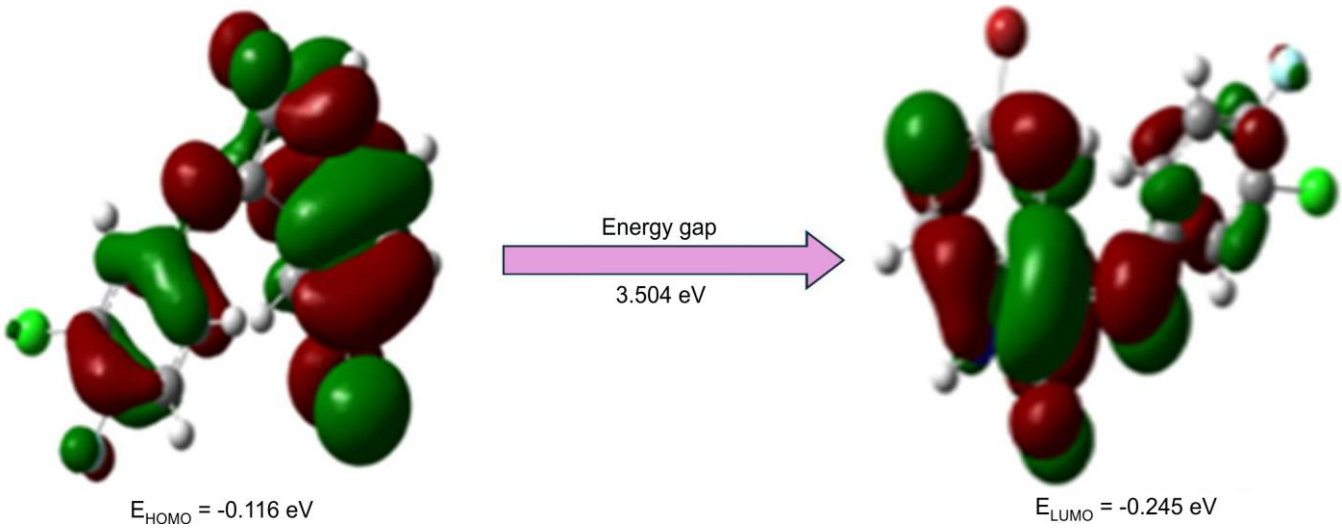

Fig. 4. HOMO-LUMO plot of 5BFIO

TABLE-4
CALCULATED BAND GAP AND
GLOBAL DESCRIPTORS VALUES OF 5BFIO

Parameters	Values
HOMO (eV)	-0.116
LUMO (eV)	-0.245
Ionization potential	0.116
Electron affinity	0.245
Energy gap(eV)	3.504
Electronegativity	0.181
Chemical potential	-0.181
Chemical hardness	-0.064
Chemical softness	-7.765
Electrophilicity index	-0.253
electronic charge	-2.804
electron donating capability (w–)	-0.171
electron accepting capability (w+)	-0.351

TABLE-5
CALCULATED DIPOLE MOMENT (D), POLARIZABILITY (α)
AND FIRST ORDER HYPERPOLARIZABILITY (β)
OF THE TITTLE COMPOUND (5BFIO)

Parameters	Values
μ (D)	2.170
α (a.u.)	224.941
α (e.s.u.)	3.333×10^{-23}
Δα (a.u.)	507.007
Δα (e.s.u.)	7.5138×10^{-23}
βtot (a.u.)	1343.594
βtot (e.s.u.)	1.1608×10^{-29}

activity. 5BFIO may be considered a highly efficacious molecule for nonlinear optical (NLO) applications.

Topological aspects: The properties of weak contacts and intermolecular interactions can be described using the non-covalent interaction index (NCI), which relies on the reduced density gradient atoms. RDG is a dimensionless parameter used as a reference tool to quantify and visualise the intense interactions of the molecule [28,29]. Electron localization function and localized orbital locator rely on the kinetic energy density. The multi-wave function programme is utilized for determining the topological parameters [30]. The ELF parameter is associated with the density of electron pairs, while the LOL parameter is linked to the localized electron cloud. Fig. 5 displays the graphical representations of the ELF and LOL in gas. The range of the electron localization function (ELF) spans from 0 to 1. A value more than 0.5 indicates the presence of bonding or anti-bonding electrons that are localized, whereas a value less than 0.5 indicates the removal of electrons. ELF investigations provide a description of the chemical structure, reactivity and bonding [31]. The compound's ELF values are determined by the colour gradient in the 2D graphical data. The red colour represents a greater ELF value, whereas the blue colour represents a lower ELF value. The electron localization function provides precise data on the localized depletion of electrons between the valence and inner shells. The blue circles indicate the presence of delocalization region carbon atoms blue (C3-C4-C5-C12).

Fig. 6 displays the RDG isosurface diagram and scattering profile of the substance in gaseous. On the *x*-axis of the diagram, $\lambda 2 < 0$ denotes bonding interactions, while $\lambda 2 > 0$ signifies non-bonding interactions. In the scattering graph, the left side indicates H-bonding (strong attraction), the right side represents steric repulsion (strong repulsion) and the middle section depicts weak van der Waals forces [32]. The RDG isosurface map vividly illustrates the steric effect, depicted by electron density depletion at the center of ring, attributed to electrostatic repulsion, indicated by the red colour. In the isosurface diagram, van der Waals forces are depicted by a disk-shaped image with green-brown colouring.

NMR analysis: Utilizing the GIAO procedure [33], the potential chemical shifts of 5BFIO were determined. Fig. 7 presents the experimental spectra equivalent to the ^{13}C and ^{1}H NMR of 5BFIO, respectively. Table-6 highlights the variations in chemical shifts, particularly for C8 and C17, measured at 113.75 and 116.41 ppm, respectively. Signals observed at 121.02 ppm are attributed to C6 and C11 (indolin ring), influenced by the presence of electronegative atoms. Computational and experimental data both indicate a chemical shift of 151.01 and 151.17 ppm for the C9 atom. Proton H27 exhibits a reduced change at 6.6 and 6.3 ppm. Signals from H atoms

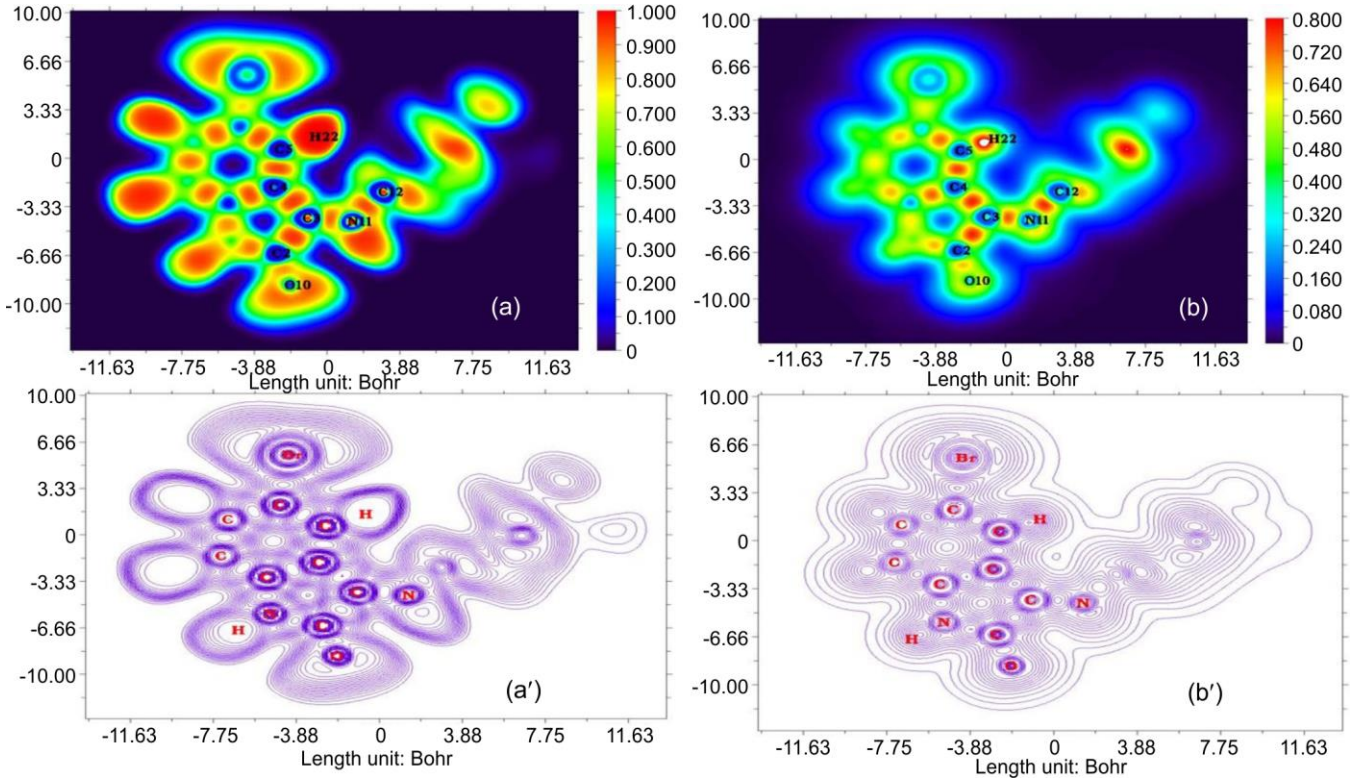

Fig. 5. ELF and LOL colour filled and contour map of 5BFIO [(a) ELF colour filled, (a') ELF contour map and (b) LOL colour filled, (b') LOL contour map)

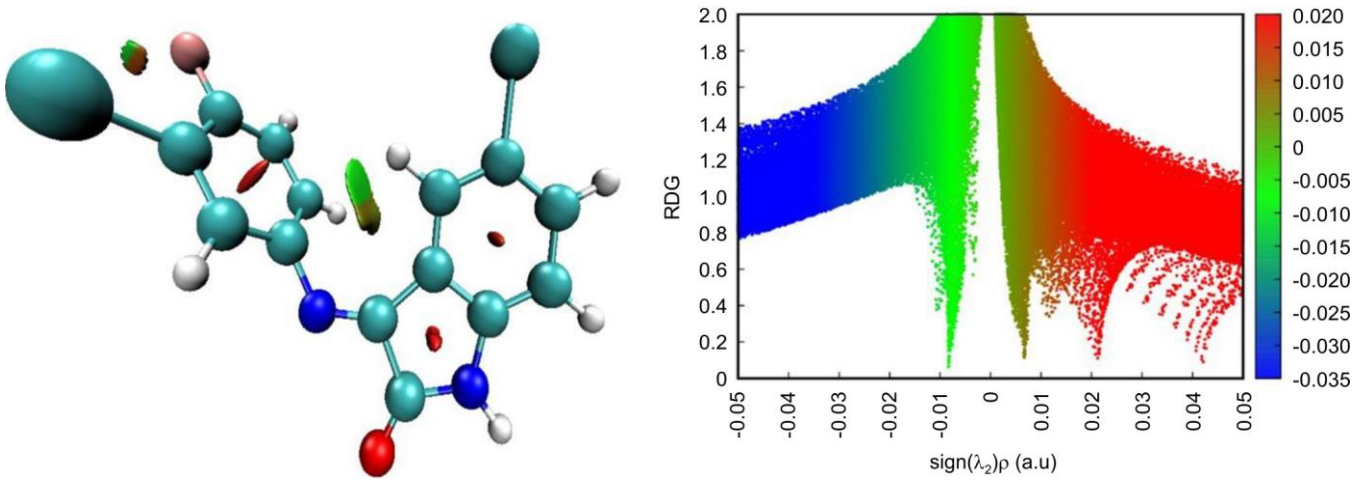

Fig. 6. NCI and RDG scatter plot of 5BFIO molecule

(H23, H22, H24 and H25) within the phenyl ring are identified at 7.35, 7.34, 7.15 and 7.27 ppm, respectively, closely matching the experimental values of 7.6, 7.3, 6.24 and 7.8 ppm. The agreement between most signals and experimental findings underscores the reliability of the computational approach.

Fukui function: The reactivity pattern of 5BFIO molecule was characterized by the Fukui function, which alternates between electrophilic and nucleophilic attacks at specific sites [34]. The Fukui function at a constant potential reveals the charge distribution in relation to the number of electrons [35]. By analyzing this function, we can predict the presence of nucleophilic and electrophilic regions within a compound. Specifically, a positive (+) Fukui factor indicates nucleophilic sites, a negative (-) factor indicates electrophilic regions and a zero (0) factor suggests areas susceptible to radial assault [36]. According to Table-7, oxygen emerges as a particularly potent electrophile. Due to the electronegativity of nitrogen, carbon becomes electron-deficient and more susceptible to nucleophilic attacks. Therefore, N1, C4, C6, C8, C9, C13, C15, C16, C17, F18, Cl19, Br20, H25, H26 and H27 act as nucleophiles, while C2, C3, C5, C7, O10, N11, C12, C14, H21, H22, H23 and H24 serve as electrophiles.

Charge transfer analysis: Investigating holes together with electrons can reveal an abundance of information on their excited electron behaviour [37]. Almost all transitions occur with the expected energies and excited states. This shows that

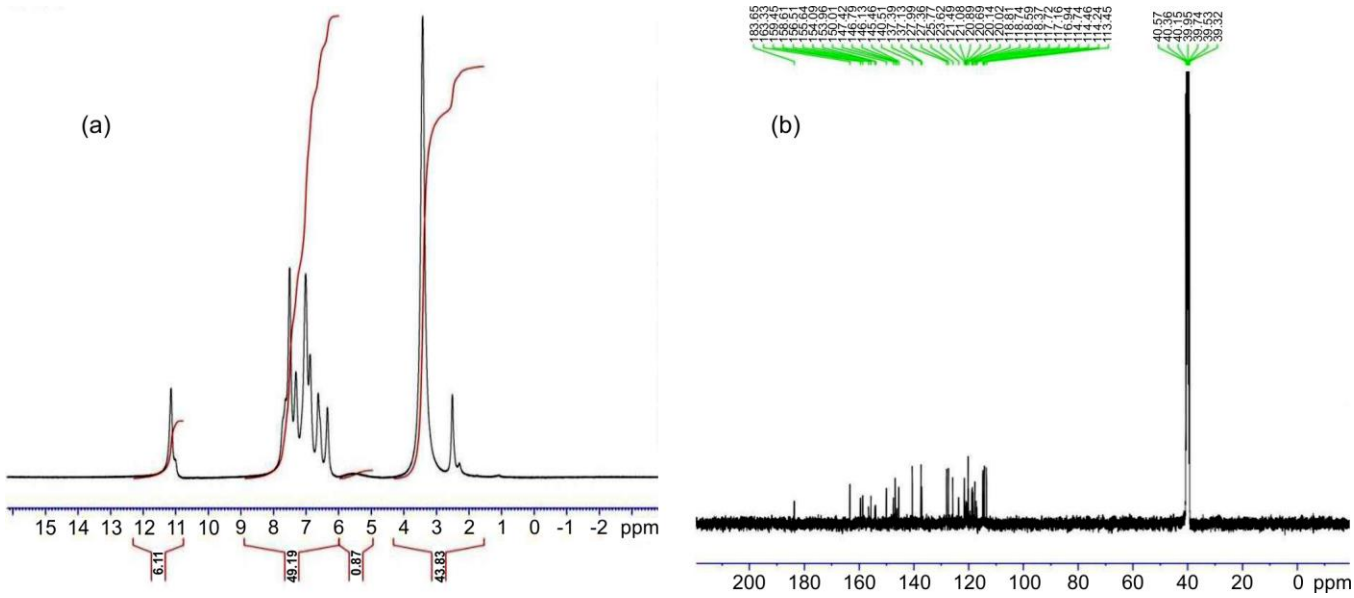

Fig. 7. (a) ^{1}H NMR and (b) ^{13}C NMR experimental spectra of 5BFIO molecule

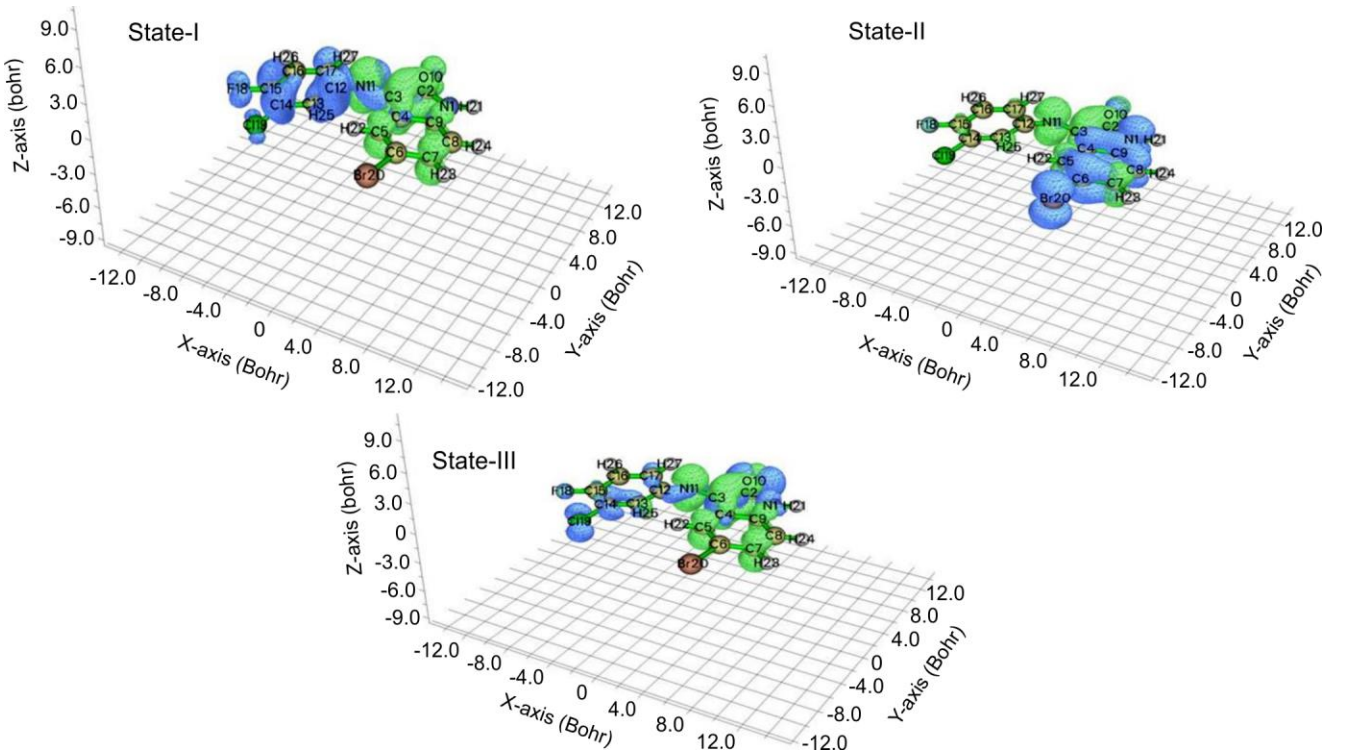

Fig. 8. Electron hole charge transfer for three excitation state of 5BFIO molecule

the levels of energy occupied by charges, in addition to the level of energy necessary to move between them, have a significant impact on their behaviour [38,39]. Table-8 show excitation energy (E), D index, Δr index, t index for different excited states. From Fig. 8 the blue shows the position of holes, whereas green denotes the position of electrons. In the 1st excited state, C and O atoms are encircled by holes, but in the 2nd and 3rd excited states, electrons encircle the ring structures. Furthermore, r is larger for a similar function, indicating that the 3rd excitation stage coincides with significant charge excitement.

Drug likeness parameters: The Lipinski rule can forecast the biological function of a molecule that has significant drug qualities and is a promising candidate for a drug [5,40]. This investigation calculates the total scoring values of a drug's similarity. Table-9 presents the drug-like properties of the 5BFIO compound showing no violations of drug-likeness criteria. Lipophilicity is an essential property that influences drug similarities. So, it is apparent that 5BFIO represents the attributes necessary for a compound to work as a drug. The results clearly indicate that 5BFIO compound possesses the necessary properties for therapeutic efficacy, confirming its bioactive potential.

TABLE-6
THEORETICAL AND EXPERIMENTAL ^{13}C AND ^{1}H ISOTOPIC CHEMICAL SHIFTS FOR 5BFIO MOLECULE

Atoms	Chemical shifts (ppm)	
	Computed	Experimental
23-H	7.35	7.6
22-H	7.34	7.3
25-H	7.27	7.8
24-H	7.15	6.54
27-H	6.6	6.3
8-C	113.75	113.43
17-C	116.41	116.91
16-C	121.02	121.79
6-C	138.57	138.69
9-C	151.01	151.7

Molecular docking: Patch dock is an online website for ligand-protein interaction [41,42]. The target proteins' structures were downloaded using the RCSB webpage [43]. Proteins were selected to investigate the anticancer capabilities of 5BFIO compound. Fig. 9 illustrates the interaction of 5BFIO ligand with each target protein, while Table-10 summarizes its binding properties. The BE for the target proteins 4B55, 5KYG and 6UGR are -5.78, -8.86 and -6.72, respectively. In contrast to other proteins, 4B55 has the most BE, whereas the 6UGR has the least BE (Table-10). The docking of these proteins to the 5BFIO demonstrates their biological role.

***In vitro* analysis:** The National Cancer Institute (NCI, USA) conducted an *in vitro* evaluation of the synthesized 5BFIO compound against 60 human carcinoma cell lines. The Developmental Therapeutics Program (DTP) assigned the code NSC: D-833718/1 to assess its cytotoxic effects. This code may be used to obtain information on 5BFIO from the NCI file, resulting in a one-dose average chart of the chemical's

TABLE-8
EXCITATION ENERGY (E), D INDEX, Δr INDEX, t INDEX FOR DIFFERENT EXCITED STATES FOR 5BFIO MOLECULE

Parameters	First excited state	Second excited state	Third excited state
Excitation energy E (eV)	2.709	2.969	3.546
Charge transfer length D index (Å)	2.743	1.912	1.379
Δr index (Å)	1.402	1.292	2.362
t index (Å)	0.925	0.145	0.526

TABLE-9
DRUG-LIKENESS PARAMETERS OF 5BFIO MOLECULE

Descriptor	Value	Falls within optimum range (Yes/No)
Hydrogen bond donors (HBD)	1	Yes
Hydrogen bond acceptors (HBA)	3	Yes
LogP	2.54	Yes
Number of atoms	20	Yes
Number of rotatable bonds	1	Yes
Molecular weight	353.6	Yes
Molar refractivity	83.13	Yes

TABLE-7
FUKUI FUNCTION AND DUAL DESCRIPTOR FOR 5BFIO MOLECULE

Atom	Mulliken atomic charges			Fukui functions			Dual descriptor
	0,1 (N)	N+1 (-1,2)	N-1 (1,2)	f_r^+	f_r^-	f_r^0	Δf(r)
1N	-0.186	-0.2	-0.145	-0.015	-0.041	-0.028	0.026
2C	0.139	0.143	0.086	0.004	0.054	0.029	-0.05
3C	-0.826	-0.894	-0.789	-0.067	-0.038	-0.052	-0.03
4C	1.992	2.006	2.017	0.014	-0.025	-0.005	0.04
5C	-1.218	-1.199	-1.273	0.02	0.054	0.037	-0.035
6C	0.094	-0.093	0.303	-0.187	-0.209	-0.198	0.022
7C	0.029	0.003	0.012	-0.026	0.017	-0.005	-0.042
8C	-0.847	-0.826	-0.851	0.021	0.004	0.013	0.016
9C	0.029	0.045	0.037	0.016	-0.008	0.004	0.024
10O	-0.305	-0.419	-0.214	-0.115	-0.091	-0.103	-0.024
11N	0.304	0.184	0.378	-0.12	-0.074	-0.097	-0.046
12C	-1.1	-1.1	-1.104	0	0.005	0.002	-0.005
13C	0.241	0.229	0.282	-0.012	-0.042	-0.027	0.03
14C	0.864	0.919	0.794	0.054	0.07	0.062	-0.016
15C	-1.081	-1.144	-1.016	-0.063	-0.065	-0.064	0.001
16C	0.105	0.08	0.132	-0.025	-0.027	-0.026	0.002
17C	0.101	0.085	0.131	-0.016	-0.03	-0.023	0.015
18F	-0.153	-0.182	-0.097	-0.03	-0.055	-0.042	0.026
19Cl	0.421	0.335	0.545	-0.086	-0.124	-0.105	0.038
20Br	-0.149	-0.251	-0.014	-0.102	-0.135	-0.119	0.033
21H	0.343	0.296	0.383	-0.047	-0.04	-0.043	-0.007
22H	0.180	0.148	0.175	-0.032	0.005	-0.013	-0.037
23H	0.233	0.181	0.275	-0.052	-0.043	-0.047	-0.009
24H	0.159	0.106	0.206	-0.053	-0.047	-0.05	-0.007
25H	0.222	0.192	0.258	-0.03	-0.036	-0.033	0.006
26H	0.221	0.185	0.266	-0.037	-0.045	-0.041	0.008
27H	0.187	0.172	0.223	-0.015	-0.036	-0.026	0.02

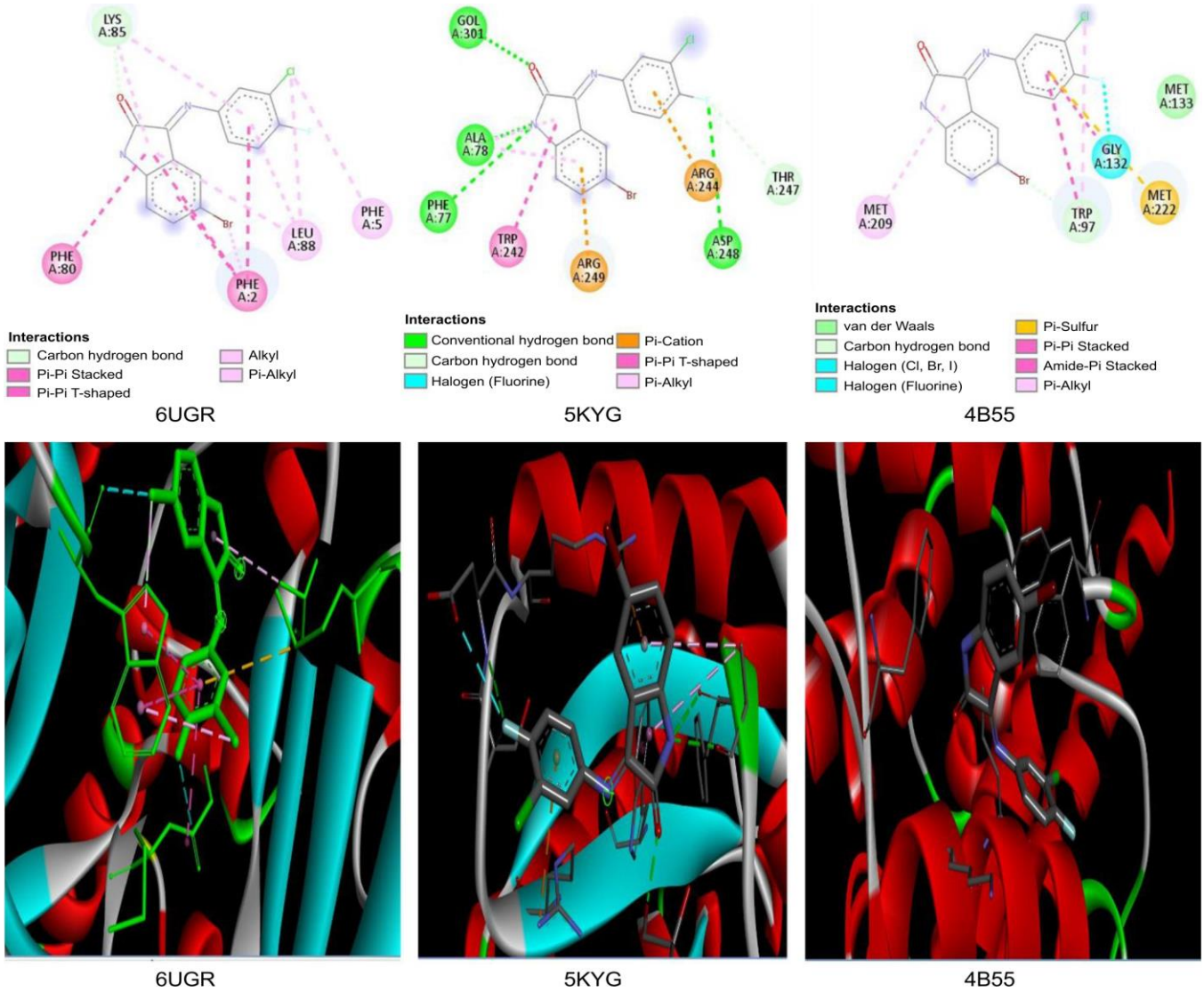

Fig. 9. Protein-Ligand interactions (2D and 3D) of 4B55, 5KYG and 6UGR with 5BFIO molecule

TABLE-10
INTERACTION ENERGY ANALYSIS OF
5BFIO MOLECULE WITH TARGETED PROTEIN

Target protein	ACE (-kcal/mol)	Inhibition constant	Interaction of 5BFI0 residue	Bond distance (Å)
4B55	-5.78	88.31	META:209	2.6
			META:133	3.3
			TRPA:97	3.6
			META:222	3.8
			GLYA:132	4.5
5KYG	-8.86	45.88	GOLA:301	3.3
			ALAA:78	2.2
			PHEA:77	2.1
			ASPA:248	3.6
			ARGA:249	3.5
			ARGA:244	4.0
			THRA:247	5.2
6UGR	-6.72	22.98	PHEA:80	4.9
			PHEA:2	4.6
			LYSA:85	3.3
			LEUA:88	5.4

percentage growth inhibition (% GI = 100 – Growth %). Fig. 10 depictone-dose mean graph for showing % GI against the 60 human cancer cell lines. According to DTP investigations, the 5BFIO did not inhibit 29 cancerous cells, although it did exhibit % GI over 31 cell types. Only CCRF-CEM cancer cells were inhibited in the leukemia panel by a synthesized hybrid oxindole-imine-containing compound that showed 8.68% GI. Similarly, EKVX, NCI-H226, NCI-H322M and NCI-H522 cancerous lines of cells were suppressed by 5BFIO and presented 8.04, 0.93, 8.72 and 6.92% GI under the non-small cell lung cancer panel, respectively. Under the sub-panel of colon cancer, five cancerous lines of cells (HCT116 and 15, KM12, HT29 and SW620) were inhibited (showed 7.41, 25.32, 11.01, 9.90 and 11.81%) GI, respectively. Five cancerous lines of cells (SF295 and SF-539, SNB-19 and 75 and U251) related to CNS were repressed and observed to be 16.96, 9.84, 11.32, 8.71 and 13.95% GI, respectively. Similarly, four tumour types of cells were reduced in the carcinoma subpanel, with % GI values of 11.09 (LOX IMVI), 2.20 (MALME-3M), 21.02 (MDA -MB-435) and 41.23 (UACC-62). Moreover, the chemical suppressed three ovarian carcinoma cells, resulting in 13.68

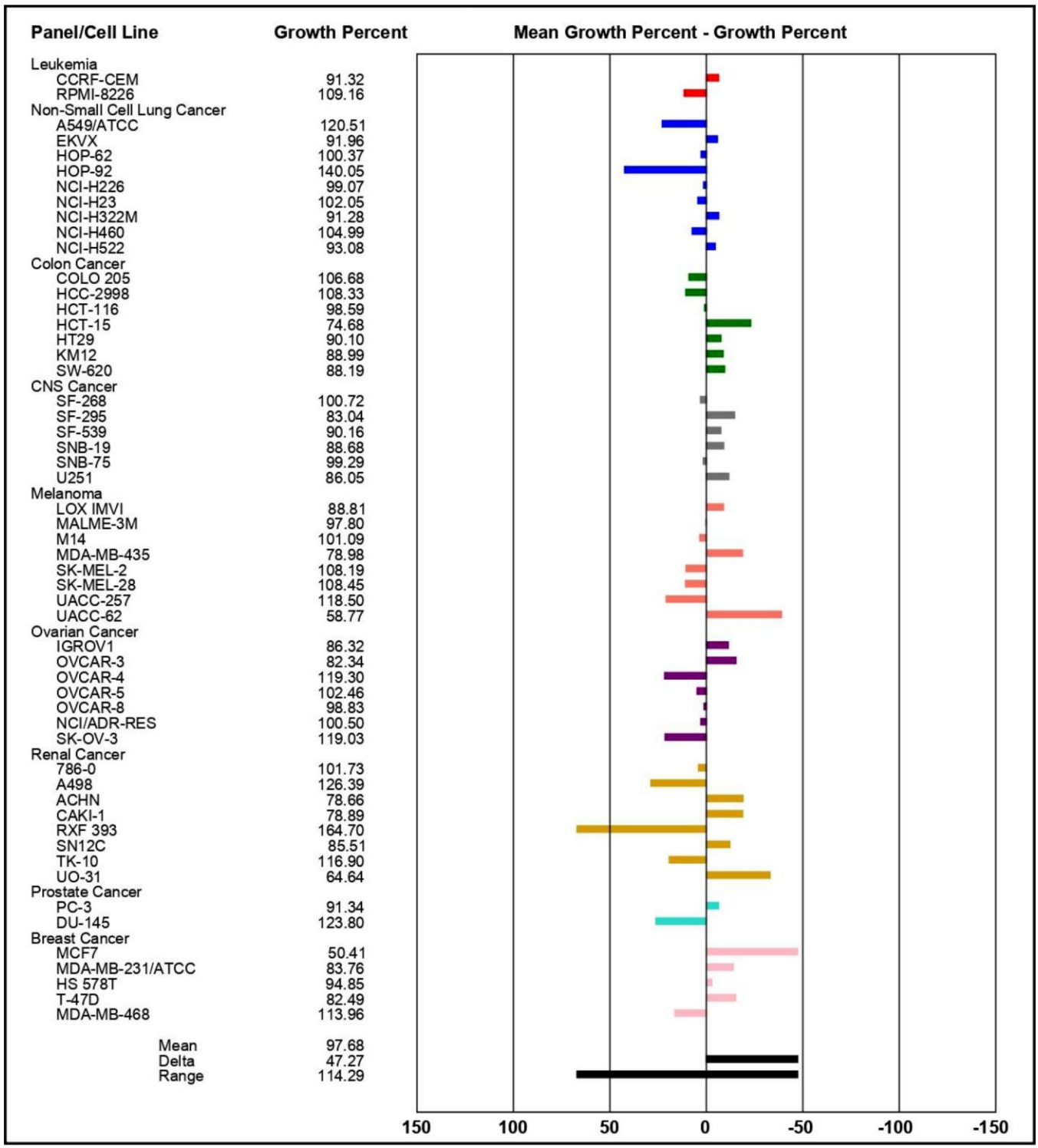

Fig. 10. One-dose mean graph for showing % GI against the sixty-human cancer cell lines

(IGROV1), 18.66 (OVCAR-3) and 1.17 (OVCAR-8) % GI, respectively. The next panel is renal cancer; fewer than four sub-panels (ACHN, CAKI-1, SN12C and UO-31) showed 21.34, 21.11, 14.49 and 35.36% GI, respectively. In the genital (prostate) tumour subpanel only the PC-3 cancer cell line was found to be 8.66% resistant to growth inhibition. The last sub-panel is coming under breast cancer. By the report, four cancerous presented 49.59 (MCF7), 16.24 (MDA-MB-231/ ATCC), 5.15 (HS 578T) and 17.51 (T-47D) % GI at 10^{-5} M, respectively. In conclusion, the proposed synthesized compound showed the best activity (49.59% GI) against the MCF7 breast cancer cell line. This compound could be derivatized to make a more potent anti-breast cancer drug.

Conclusion

The theoretical validation of the imine-containing hybrid 5BFIO was investigated and the theoretical analysis, which

included FT-Raman, FT-IR, ^{1}H and ^{13}C NMR, confirmed their analytical values. With the help of PED, all the functional groups were found after a thorough analysis. The MEP map of 5BFIO was used to find more reacting sites, electrophilic areas and nucleophilic areas. To investigate electronic variations, the highest band gap energy was observed in the gas phase, consistent with the band gap obtained from FMO analysis. The HOMO–LUMO analysis in the gas phase was used to evaluate the chemical reactivity and stability of 5BFIO. The FMO study provided essential theoretical support, confirming the molecule's biological activity and non-toxic nature. Moreover, the theoretical and experimental chemical shifts for carbon and hydrogen atoms were estimated and compared. Electron density analysis was conducted to identify the electronegative regions within the 5BFIO structure. As a result, the structure of 5BFIO was tested for its antitumor efficacy over sixty lines of malignant human cells. Anticancer activity of 5BFIO against 4B55, 5KYG and 6UGR proteins was demonstrated by employing molecular linking as an initial investigation, which revealed that the interaction with the ligand has considerable binding affinity of -5.78, -8.86 and -6.72 kcal/mol, respectively. Drug-likeness, binding energies of docked complexes and anticancer activity suggested that it could be used for *in vivo* analysis to assess their cytotoxicity.

CONFLICT OF INTEREST

The authors declare that there is no conflict of interests regarding the publication of this article.

REFERENCES

1. M. Fatma, S. Parveen and S.S. Mir, *Biochim. Biophys. Acta Rev. Cancer*, **1880**, 189309 (2025); https://doi.org/10.1016/j.bbcan.2025.189309
2. I. Azad, P. Anand, N. Ahmad, F. Hassan, M. Faiyyaz and Y. Akhter, *Chem. Phys.*, **581**, 112243 (2024); https://doi.org/10.1016/j.chemphys.2024.112243
3. M. Asif, T. Azaz, B. Tiwari and M. Nasibullah, *Tetrahedron*, **134**, 133308 (2023); https://doi.org/10.1016/j.tet.2023.133308
4. V.J. Reeda, V.B. Jothy, M. Asif, M. Nasibullah, S. Kadaikunnan, G. Abbas and S. Muthu, *J. Mol. Struct.*, **1294**, 136310 (2023); https://doi.org/10.1016/j.molstruc.2023.136310
5. V.S. Jeba Reeda, V. Bena Jothy, M. Asif, M. Nasibullah, N.S. Alharbi, G. Abbas and S. Muthu, *J. Mol. Liq.*, **380**, 121709 (2023); https://doi.org/10.1016/j.molliq.2023.121709
6. M. Asif, M. Saquib, A.R. Khan, F. Aqil, A.S. Almalki, F.A. Alasmary, J. Singh and M. Nasibullah, *ChemistrySelect*, **8**, e202204536 (2023); https://doi.org/10.1002/slct.202204536
7. M.J. Frisch, G.W. Trucks, H.B. Schlegel, G.E. Scuseria, M.A. Robb, J.R. Cheeseman, G. Scalmani, V. Barone, B. Mennucci, G.A. Petersson, H. Nakatsuji, M. Caricato, X. Li, H.P. Hratchian, A.F. Izmaylov, J. Bloino, G. Zheng, J.L. Sonnenberg, M. Hada, M. Ehara, K. Toyota, R. Fukuda, J. Hasegawa, M. Ishida, T. Nakajima, Y. Honda, O. Kitao, H. Nakai, T. Vreven, J.A. Montgomery Jr., J.E. Peralta, F. Ogliaro, M. Bearpark, J.J. Heyd, E. Brothers, K.N. Kudin, V.N. Staroverov, R. Kobayashi, J. Normand, K. Raghavachari, A. Rendell, J.C. Burant, S.S. Iyengar, J. Tomasi, M. Cossi, N. Rega, J.M. Millam, M. Klene, J.E. Knox, J.B. Cross, V. Bakken, C. Adamo, J. Jaramillo, R. Gomperts, R.E. Stratmann, O. Yazyev, A.J. Austin, R. Cammi, C. Pomelli, J.W. Ochterski, R.L. Martin, K. Morokuma, V.G. Zakrzewski, G.A. Voth, P. Salvador, J.J. Dannenberg, S. Dapprich, A.D. Daniels, Ö. Farkas, J.B. Foresman, J.V. Ortiz, J. Cioslowski and D.J. Fox, Gaussian 09, Revision D.01, Gaussian Inc., Wallingford CT (2009).
8. R. Dennington, T.A. Keith and J.M. Millam, GaussView 6.0. 16. Semichem Inc.: Shawnee Mission, KS, USA (2016).
9. R. Krishnan, J.S. Binkley, R. Seeger and J.A. Pople, *J. Chem. Phys.*, **72**, 650 (1980); https://doi.org/10.1063/1.438955
10. M.H. Jamróz, *Spectrochim. Acta A Mol. Biomol. Spectrosc.*, **114**, 220 (2013); https://doi.org/10.1016/j.saa.2013.05.096
11. I.M. Alecu, J. Zheng, Y. Zhao and D.G. Truhlar, *J. Chem. Theory Comput.*, **6**, 2872 (2010); https://doi.org/10.1021/ct100326h
12. G.A. Andrienko, Chemcraft-Graphical Software for Visualization of Quantum Chemistry Computations, Version 1.8, build 648 (2015).
13. P. Politzer and D.G. Truhlar, Chemical Applications of Atomic and Molecular Electrostatic Potentials: Reactivity, Structure, Scattering, and Energetics of Organic, Inorganic and Biological Systems, Springer Science & Business Media (2013).
14. R.S. Mulliken, *J. Chem. Phys.*, **2**, 782 (1934); https://doi.org/10.1063/1.1749394
15. A.E. Reed, L.A. Curtiss and F. Weinhold, *Chem. Rev.*, **88**, 899 (1988); https://doi.org/10.1021/cr00088a005
16. T. Lu and F. Chen, *J. Comput. Chem.*, **33**, 580 (2012); https://doi.org/10.1002/jcc.22885
17. A. Daina, O. Michielin and V. Zoete, *Sci. Rep.*, **7**, 42717 (2017); https://doi.org/10.1038/srep42717
18. D. Schneidman-Duhovny, Y. Inbar, R. Nussinov and H.J. Wolfson, *Nucleic Acids Res.*, **33(Web Server)**, W363 (2005); https://doi.org/10.1093/nar/gki481.
19. C.P.S. Hsu, Infrared Spectroscopy, In: Handbook of Instrumental Techniques for Analytical Chemistry. Prentice-Hall, Englewood Cliffs, NJ, pp. 247-284 (1997).
20. P. Mishra, A. Behera, D. Kandi and K. Parida, *Nanoscale Adv.*, **1**, 1864 (2019); https://doi.org/10.1039/C9NA00018F
21. A. McIlroy and D.J. Nesbitt, *J. Chem. Phys.*, **91**, 104 (1989); https://doi.org/10.1063/1.457496
22. B.Q. Sheeba, M.S. Michael Mary, M. Amalanathan and C.B. Job, *Mol. Simul.*, **47**, 1217 (2021); https://doi.org/10.1080/08927022.2021.1962862
23. L. Kahovec and K.W.F. Kohlrausch, *Monatsh. Chem.*, **74**, 333 (1941); https://doi.org/10.1007/BF01512909
24. P. Manikandan, M. Kumar, P. Swarnamughi, M. Asif, M. Nasibullah, V.S. Jeba Reeda, J.M. Khaled and S. Muthu, *J. Mol. Liq.*, **405**, 125064 (2024); https://doi.org/10.1016/j.molliq.2024.125064
25. G. Kanimozhi, S. Tamilselvan, K.M. Potla, J.N. Cheerlin Mishma, F. Akman, M. Vimalan, N.S. Alharbi, G. Abbas and S. Muthu., *J. Mol. Liq.*, **391**, 123368 (2023); https://doi.org/10.1016/j.molliq.2023.123368
26. S. Selvakumar, A. Prabakaran, P. Manikandan and M. Nikpassand, *Biochem. Biophys. Res. Commun.*, **770**, 151989 (2025); https://doi.org/10.1016/j.bbrc.2025.151989
27. M. Essid, S. Muhammad, H. Marouani, A. Saeed, Z. Aloui and A.G. Al-Sehemi, *J. Mol. Struct.*, **1211**, 128075 (2020); https://doi.org/10.1016/j.molstruc.2020.128075
28. K. Arulaabaranam, S. Muthu, G. Mani and A. Irfan, *J. Mol. Liq.*, **341**, 116934 (2021); https://doi.org/10.1016/j.molliq.2021.116934
29. S. Janani, H. Rajagopal, S. Muthu, S. Aayisha and M. Raja, *J. Mol. Struct.*, **1230**, 129657 (2021); https://doi.org/10.1016/j.molstruc.2020.129657
30. N. Elangovan, R. Sangeetha, S. Sowrirajan, S. Sarala and S. Muthu, *Anal. Chem. Lett.*, **12**, 58 (2022); https://doi.org/10.1080/22297928.2021.1933588
31. F. Basha, F.L.A. Khan, S. Muthu and M. Raja, *Comput. Theor. Chem.*, **1198**, 113169 (2021); https://doi.org/10.1016/j.comptc.2021.113169
32. A. Irfan, M. Hussien, A.R. Chaudhry, M.A. Qayyum, A.G. Al-Sehemi, S. Selvakumari and S. Muthu, *J. Mol. Liq.*, **390**, 122956 (2023); https://doi.org/10.1016/j.molliq.2023.122956

33. R. Laskowski, P. Blaha and F. Tran, *Phys. Rev. B Condens. Matter Mater. Phys.*, **87**, 195130 (2013); https://doi.org/10.1103/PhysRevB.87.195130
34. V. Pilepić and S. Uršić, *J. Mol. Struct. THEOCHEM*, **538**, 41 (2001); https://doi.org/10.1016/S0166-1280(00)00642-4
35. A.D. Isravel, J.K. Jeyaraj, S. Thangasamy and W.J. John, *Comput. Theor. Chem.*, **1202**, 113296 (2021); https://doi.org/10.1016/j.comptc.2021.113296
36. A. Bendjeddou, T. Abbaz, A. Gouasmia and D. Villemin, *Int. Res. J. Pure Appl. Chem.*, **12**, 1 (2016); https://doi.org/10.9734/IRJPAC/2016/27066
37. A. Fatima, G. Khanum, I. Verma, R.J. Butcher, N. Siddiqui, S.K. Srivastava and S. Javed, *Polycycl. Aromat. Compd.*, **43**, 1644 (2023); https://doi.org/10.1080/10406638.2022.2032769
38. M. Timmer and P. Kratzer, *Phys. Rev. B Condens. Matter Mater. Phys.*, **79**, 165407 (2009); https://doi.org/10.1103/PhysRevB.79.165407
39. J.J. Bhargiri, S.C. Parakkal, R. Datta, N.S. Alharbi, S. Kadaikunnan and S. Muthu, *Comput. Theor. Chem.*, **1237**, 114649 (2024); https://doi.org/10.1016/j.comptc.2024.114649
40. C.S. Abraham, S. Muthu, J.C. Prasana, S. Armaković, S.J. Armaković, F. Rizwana B, B. Geoffrey and H.A. David R, *Spectrochim. Acta A Mol. Biomol. Spectrosc.*, **222**, 117188 (2019); https://doi.org/10.1016/j.saa.2019.117188
41. N. Agarwal, I. Verma, N. Siddiqui and S. Javed, *J. Mol. Struct.*, **1245**, 131046 (2021); https://doi.org/10.1016/j.molstruc.2021.131046
42. N. Issaoui, H. Ghalla, F. Bardak, M. Karabacak, N. Aouled Dlala, H.T. Flakus and B. Oujia, *J. Mol. Struct.*, **1130**, 659 (2017); https://doi.org/10.1016/j.molstruc.2016.11.019
43. P.W. Rose, A. Prlić, A. Altunkaya, C. Bi, A.R. Bradley, C.H. Christie, L. Di Costanzo, J.M. Duarte, S. Dutta, Z. Feng, R.K. Green, D.S. Goodsell, B. Hudson, T. Kalro, R. Lowe, E. Peisach, C. Randle, A S. Rose, C. Shao, Y.-P. Tao, Y. Valasatava, M. Voigt, J.D. Westbrook, J. Woo, H. Yang, J.Y. Young, C. Zardecki, H.M. Berman and S.K. Burley, *BMC Cancer*, **16**, 77 (2016); https://doi.org/10.1186/s12885-016-2082-y